Acta Geodyn. Geomater., Vol. 23, No. 1 (221), 85–98, 2026
DOI: 10.13168/AGG.2026.0005
journal homepage: https://www.irsm.cas.cz/acta

ORIGINAL PAPER

MAPPING HYDROTHERMAL ALTERATION ZONES USING LANDAST 9 MULTISPECTRAL IMAGERY IN THE TATA REGION, SOUTHEASTERN ANTI-ATLAS, MOROCCO

Mohamed BERAAOUZ [1, 2] *, Khalid HAMMA [3], Abderrahmen CHAHBOUN [3], Nasser BOUCHIBA [3], Jijun MENG [3], Mohammed HSSAISOUNE [1, 2] and Mohammed El HAFYANI [1]

[1] *Applied Geology and Geo-Environment Laboratory, Faculty of Sciences, Ibn Zohr University, Agadir, Morocco*
[2] *Faculty of Applied Sciences, Ibn Zohr University, Ait Melloul, Morocco*
[3] *Silk Road Mineral Exploration SARL, Rabat, Morocco*

**Corresponding author's e-mail:* m.beraaouz@uiz.ac.ma; mberaaouz@gmail.com

ARTICLE INFO

Article history:
Received 20 November 2025
Accepted 16 January 2026
Available online 30 January 2026

Keywords:
Tata
Landsat 9
Hydrothermal mineralization
Iron oxide

AA

ABSTRACT

This study investigates the potential of multispectral remote sensing data, specifically Landsat 9 imagery, to map hydrothermal alteration zones in the Tata region, located in the southeastern Anti-Atlas of Morocco. The research focuses on identifying iron oxide and hydrothermal alteration zones using advanced image processing techniques, including Principal Component Analysis (PCA), band ratios, and spectral indices. The methodology also incorporates directional filters for lineament extraction and field validation to ensure accuracy. The PCA approach effectively reduced data dimensionality while enhancing relevant spectral features, particularly those indicative of iron oxide and hydrothermal mineralization. Band ratios and spectral indices further delineated iron oxide and hydrothermal alteration areas, which were corroborated by field investigations revealing polymetallic mineralization, including copper, lead, and iron oxides. The results highlight the strong structural control on mineralization and demonstrate the usefulness of multispectral remote sensing for regional mineral exploration. Field validation based on approximately 38 mineralized observation points shows a strong spatial coincidence between mapped alteration zones and known surface mineralization.

1. INTRODUCTION

In recent decades, remote sensing techniques have become valuable tools for mineral exploration, serving as an effective preliminary step for geological investigations by providing a synoptic view of large and often inaccessible areas (Kariuki et al., 2004; Peña and Abdelsalam, 2006; Adiri et al., 2020; Pour et al., 2018; Pour et al., 2023; Hajaj et al., 2024). Following the launch of the first Earth observation satellites in the early 1970s, multispectral sensors have enabled cost-effective, regional-scale investigation of surface geological features (Hajaj et al., 2024). These technologies are particularly useful for detecting hydrothermal alteration signatures that act as surface indicators of mineralized systems, especially in arid and structurally complex regions.

Remote sensing has proven that it is a helpful tool in detecting alteration zones and, consequently, minerals explorations and used in the field of geological and structural mapping (El Atillah et al., 2019; Bahrami et al., 2021; Pour and Hashim, 2015; Adiri et al., 2016). These involve extracting information about the mineral alteration using multispectral and hyperspectral satellite image processing (Adiri et al., 2016; Mamouch et al., 2022). It allows geologists working in extended areas that are usually inaccessible to study, by collecting data in different spectral bands (such as visible, infrared and microwave) (Pour et al., 2016; Pour et al., 2018; Rawan et al., 2003). This considerably improves the efficiency, precision and coverage of geological surveys, making them an essential tool in the field (Safari et al., 2018).

In addition, remote sensing and satellite image processing has been used largely in mining prospecting (Benaissi et al., 2022; Adiri et al., 2020), lithological and geological survey (Mamouch et al., 2021; Lamrani et al., 2021; Chakouri et al., 2020; Jellouli et al., 2019) structure (faults, folds, fractures) mapping (Zafaty et al., 2023; El Aoufir et al., 2024; Chakouri et at., 2022), and lineaments extraction (Das et al., 2009; Ahmed Iiand Mansor, 2018; Chaves et al., 2020; Adiri et al., 2017; Jellouli et al., 2021; Si Mhamdi et al., 2017). Especially hydrothermal alteration mapping, which has received particular attention due to its potential economic implications (Mamouch et al., 2022; Abrams et al., 1977; Abrams et al., 1983; Goetz et al., 1983; Kruse et al., 1993; Rowan et al., 1977; Adiri et al., 2018). And therefore, the use of spectral satellite imagery makes it possible to produce a geological map of different types of alteration, such as iron oxide and hydrothermal alteration zones (Zhang et al., 2007).

Cite this article as: Beraaouz M, Hamma K, Chahboun A, Bouchiba N, Meng J, Hssaisoune M, El Hafyani M: Mapping hydrothermal alteration zones using Landast 9 multispectral imagery in the Tata region, Southeastern Anti-Atlas, Morocco. Acta Geodyn. Geomater., 23, No. 1 (221), 85–98, 2026. DOI: 10.13168/AGG.2026.0005

In Morocco, several works were carried out in the domain of remote sensing in geological applications. In 2021, Mamouch et al. carried out a study with the objective of the use of a combined approach of remote sensing technique, GIS, and fuzzy logic modeling to map the hydrothermal alteration zones in the Eastern Anti-Atlas, Morocco. The results showed a spatial correlation between the extracted favorable zones and mineral occurrences. In similar context, the Landsat 8 OLI images were used to map the lithological, geological structures, and hydrothermal alteration zones in Jbel Boulachral, Eastern Anti-Atlas, Morocco (Courba et al., 2023). In this study, the band ratio, the principal component analysis, and the composite ratios were used. The results showed that high lineaments density areas are correlated with the areas with the high mineralization occurrences, and those with hydrothermal alteration.

As known, The Anti-Atlas Mountain range constitutes a significant metallogenic province, characterized by abundant polymetallic mineralization, including economically important copper, silver, cobalt, and lead deposits. In this work, the Landsat 9 image was used to map the hydrothermal alteration zones, and the geological structures. For this purpose, the techniques used, including the band ratio, the principal component analysis, directional filters, and the lineaments extraction. Then, the results were validated using field investigations.

Despite the recognized metallogenic potential of the Anti-Atlas, the systematic use of Landsat 9 multispectral imagery for hydrothermal alteration mapping in the Tata region remains unexplored. This study aims to: (i) evaluate the capability of Landsat 9 data to map iron oxide and hydrothermal alteration zones in the Tata region; (ii) integrate structural lineament analysis with alteration mapping to assess the structural control of mineralization; and (iii) validate the remote-sensing-derived targets through field observations of polymetallic mineralization. By combining spectral analysis, structural interpretation, and field verification, this work advances beyond previous regional studies and provides a new framework for mineral exploration in arid environments.

2. MATERIALS AND METHODS

2.1. GEOLOGICAL SETTING

The Anti-Atlas is a mountain chain that forms a vast anticlinal bulge-oriented ENE-WSW at the northern edge of the West African Craton (WAC) (Fig. 1). It consists of a Proterozoic basement exposed in the inliers, under a late Precambrian to Paleozoic sedimentary cover. This Anti-Atlas Range of Morocco comprises ca. 24,000 km2 of surface exposures of Ordovician rocks (Gutiérrez-Marco et al., 2019), that are very mineralized with different types of mineralization namely ferruginous mineralization, copper and lead.

The Ordovician succession is subdivided into a series of lithostratigraphic units in the Anti-Atlas region (Choubert, 1943; Choubert and Termier, 1947; Destombes, 1971; Destombes et al., 1985):

- Outer Feijas Shale Group (Tremadocian–Darriwilian): Comprising the lower/upper Fezouata and Tachilla formations, characterized by graptolite-bearing siltstones with some thin sandstone interbeds.
- First Bani Group (Darriwilian–Sandbian): A thick, extensive sandstone-dominant unit subdivided into five formations (Taddrist, Bou Zeroual, Guezzart, Ouine-Inirne, and Izegguirene).
- Ktaoua Group (Sandbian–Katian): A sequence of shale-dominant units (Lower and Upper Ktaoua) separated by the sandstone-rich Upper Tiouririne Formation.
- Second Bani Group (Hirnantian): A glaciogenic succession infilling Hirnantian paleoreliefs, marking the end of the Ordovician period (Sumrall and Zamora, 2011; Lefebvre et al., 2015; Álvaro et al., 2022).

The Paleozoic cover of the Anti-Atlas constitutes a major metallogenic province, notable for its significant copper mineralization. More than 200 copper occurrences have been identified (Bouchta et al., 1977), several of which are currently being exploited (Oummouch et al., 2017). The main deposits of the western Anti-Atlas include the world-class Cu–Ag Tizert deposit, together with the Tazalaght, Ouansimi, and Agoujgal deposits. These mineralizations occur either as stratiform bodies hosted within Lower Cambrian detrital and carbonate formations or as vein-type ores controlled by faults and fractures related to Hercynian deformation (Oummouch et al., 2017; El Basbas et al., 2020; Ouchchen et al., 2021; Askkour et al., 2023; El Ouad et al., 2025).

Ferruginous mineralization is also widespread within Ordovician outcrops across the Anti-Atlas, where it forms sedimentary lens-shaped layers in various formations specifically at the base of the Upper Fezouata Formation (Floian age), the Tachilla Formation (Dapingian age), and the Premier Bani Formation (Darriwilian age). The best-known example is the Toughza deposit (Broothaers, 1977; Raddi et al., 2011; Abia et al., 2020).

In contrast, lead and copper mineralizations occur mainly as hydrothermal veins, such as the lead mineralization at Jbel Addana (Desthieux, 1977) and the copper mineralization at the Oumjrane Bou Nahas mine (Kharis et al., 2011). The present study focuses on the field validation of remote sensing techniques for detecting alteration zones associated with hydrothermal mineralization in Tata, Foum Zguid and Fam El Hisn areas (Fig. 1).

2.2. TECTONIC SETTING

The Hercynian orogeny, a consequence of the Late Paleozoic Variscan collision between Laurasia and Gondwana, is the principal deformation observed

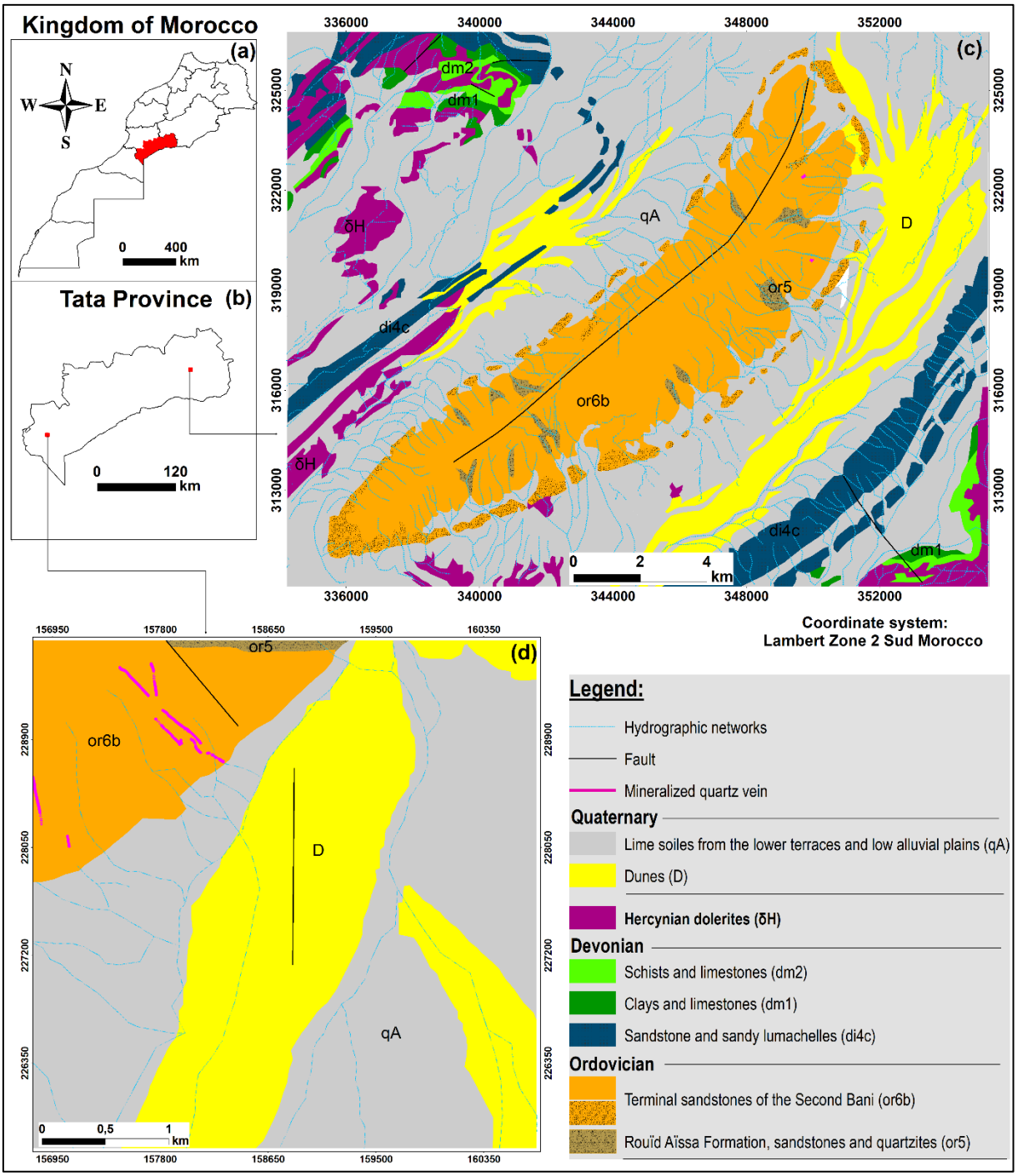

Fig. 1 (a) Moroccan boundaries and location of Tata Province; (b) Location of the studied areas in Tata Province territory; (c) Simplified geological map of the Fam El Hisn mining area; Simplified geological map of the Foum Zguid mining area.

in the Paleozoic cover of the Anti-Atlas (Choubert, 1963; Mattauer et al., 1972; Hassenforder, 1987). This deformation is generally moderate and manifests as a series of folds whose axial trends rotate systematically from a predominant NE-SW orientation in the western Anti-Atlas to a NW-SE direction in the east (Choubert, 1963; Donzeau, 1974; Piqué and Michard, 1981; Faik, 2005).

The structural style is predominantly thick-skinned and results from the compressional reactivation of inherited Precambrian fault systems, which have controlled the tectono-sedimentary evolution of the region since the Neoproterozoic (Hassenforder, 1987; Soulaimani, 1997; Michard et al., 2008). These long-lived structures were reactivated mainly as reverse and strike-slip faults (Piqué et al., 1995), leading to differential uplift of basement blocks and deformation of the overlying sedimentary cover. Locally, thin-skinned deformation is observed in the western Anti-Atlas and is

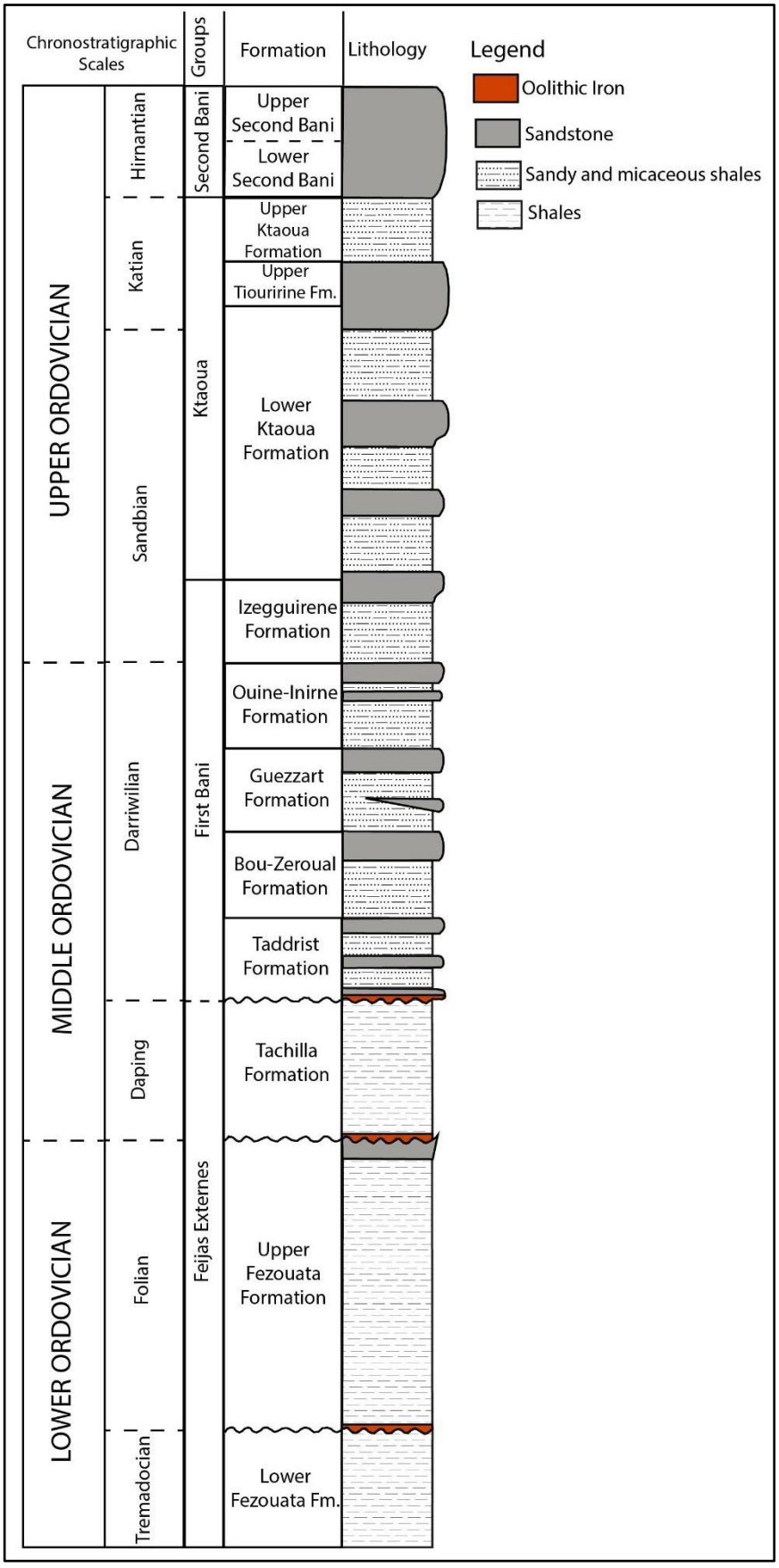

Fig. 2 Ordovician stratigraphic subdivisions of the Anti-Atlas (modified from (Destombes, 1963; Destombes et al., 1985; Gutiérrez-Marco et al., 2003; Villas et al., 2006; Sumrall and Zamora, 2011; Lefebvre et al., 2015; Javier Álvaro et al., 2022).

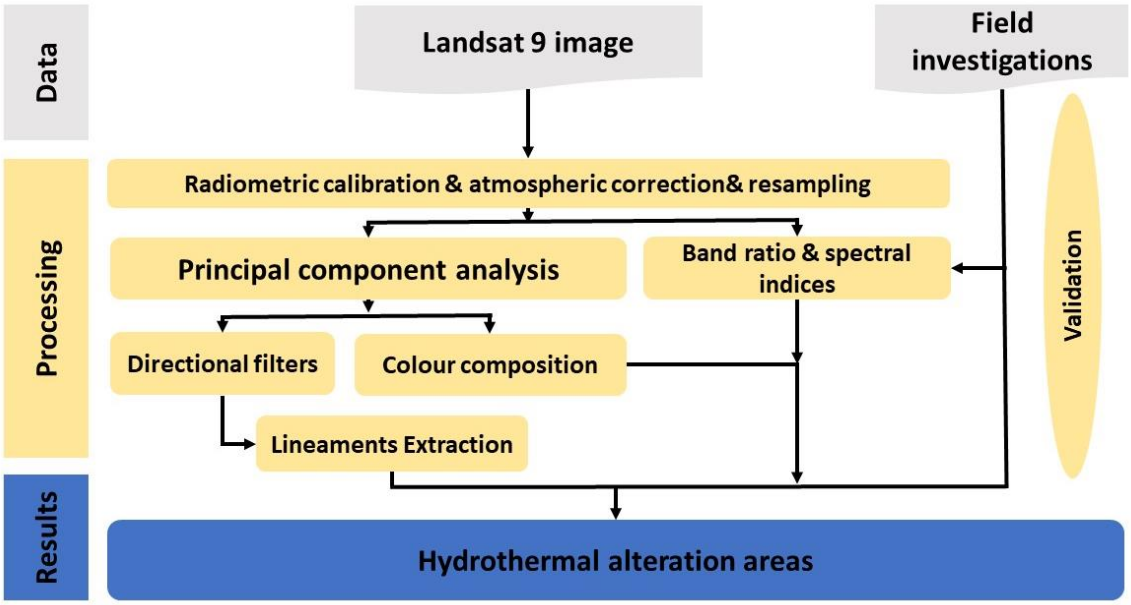

Fig. 3 Flowchart of the adopted methodology.

characterized by ESE-verging thrusts associated with more intense folding of the adjacent sedimentary cover (Belfoul et al., 2001; Soulaimani et al., 1997).

The Anti-Atlas as a whole experienced regional NW-SE shortening, accommodated by both thrust and strike-slip faulting. The resulting Hercynian folds exhibit a clear spatial variation in axial orientation: NE-SW to N–S in the west, WNW-ESE in the central region, and NW-SE in the east (Faik, 2005), (Michard et al., 2008), (Soulaimani et al., 2014). This pattern reflects a regional structural framework whose heterogeneity is fundamentally controlled by the contrasting geometry of the reactivated Precambrian basement blocks (Soulaimani and Burkhard, 2008).

2.3. METHODOLOGY

A multispectral image from the Landsat 9 satellite Level 1, acquired on August 15, 2024, with the information's (path 202, row 40, cloud cover 0 %), was downloaded from the U.S. Geological Survey's Earth Explorer platform (https://earthexplorer.usgs.gov/ (accessed on October 19, 2024)). The initial dataset features spectral bands from the visible to thermal infrared range at a 30-meter spatial resolution. Image preprocessing, bands ratio and indices calculations, as well as PCA extraction, were performed using the Semi-Automatic Classification Plugin in QGIS software. Subsequently, ArcMap was employed to filter false faults. Preprocessing steps consisted of radiometric calibration and atmospheric correction using Dark Object Subtraction (DOS) algorithm. This technique starts with the assumption that there is a high probability that there are at least some pixels in an image that should be black (0 % reflectance). The resolution was subsequently improved to 15 meters via a pan-sharpening algorithm, which integrates the multispectral information with the native 15-meter panchromatic band. From the preprocessed image, we extracted Principal Component Analysis (PCA) bands and computed spectral indices sensitive to iron oxide alteration. To enhance linear structural features, directional filters with 3×3 and 5×5 kernel sizes were applied, and a lineament map was automatically and/or manually delineated. The remote sensing results were rigorously validated against field observations. Subsequently, all data were synthesized to perform a general geological and structural analysis of the study area (Fig. 3).

2.3.1. PRINCIPAL COMPONENT ANALYSIS

The principal components (PCs) transformation is a multivariate statistical technique for reducing the dimensionality of large datasets while retaining as much variability (information) as possible. It has been successfully applied to the identification of anomalous concentrations in mining exploration (El Atillah et al., 2019; Loughlint, 1991). The Crosta technique developed by Crosta and Moore in 1989 to identify areas of mineral alteration associated with hydrothermal processes. This method is recognized as a feature-oriented approach to PC selection, it highlights areas where materials appear as bright or dark pixels in the principal components (Ranjbar et al., 2004). The application of PCA technique and the color composite of PCA has allowed the hydrothermal alteration of minerals and iron oxide extraction.

2.3.2. BAND RATIO AND SPECTRAL INDICES

Band ratios and spectral indices are a commonly used technique in remote sensing to highlight specific features in multispectral imagery by dividing the reflectance values of one spectral band by those of another, or by using some mathematical formula using the high and the low reflectance band value. These techniques were validated and showed their

Table 1 Spectral band ratios of Landsat 9 (Ito et al., 2022; Sabins, 1999).

Mineral	Band Ratio	Description
Iron Minerals	4/2	Ferric Iron
Iron Minerals	(4/2)*((4+6)/5)	Ferric Iron
Iron Minerals	(3+6)/(4+5)	Ferrous Iron, coarsed grained ferric iron
Sulfates	(2/1)-(5/4)	Iron sulphate

Table 2 EigenValue of PCA.

PCA	PC_1	PC_2	PC_3	PC_4	PC_5	PC_6	PC_7
Eigenvalues	**99.121**	**0.648**	**0.175**	**0.037**	**0.016**	**0.004**	**0.000**

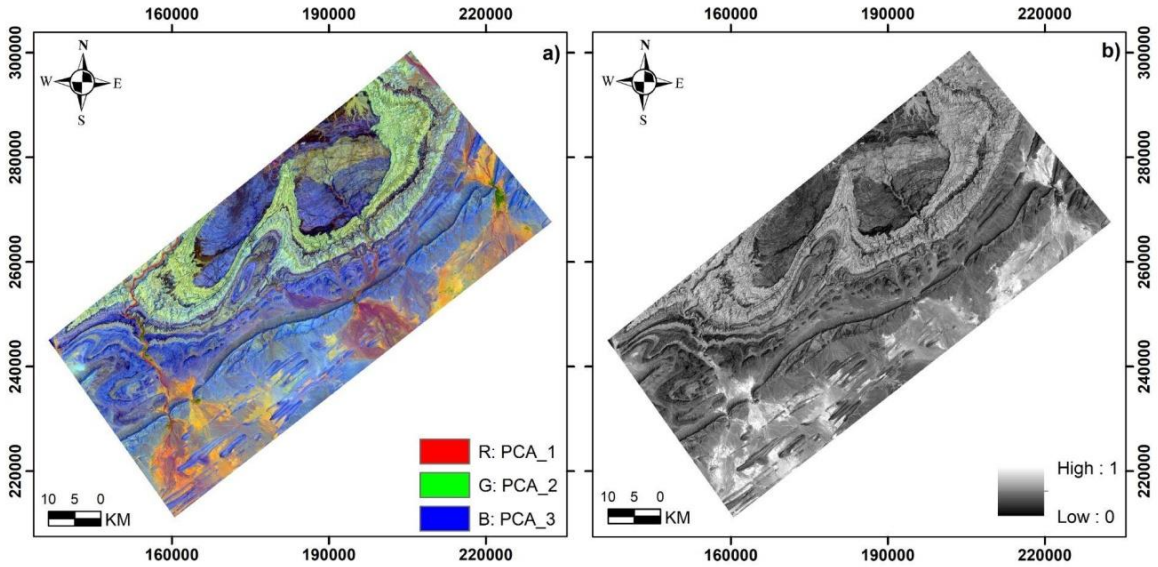

Fig. 4 a) Color composition of PC-1, PC-2, PC-3, b) Grey scale of PC-1.

effectiveness, especially in lithological and mineralogical mapping (Choukrad et al., 2023; Adiri et al., 2016). This method makes it possible to highlight the subtle differences in the spectral reflectance of specific elements or materials that may not be visible in the raw spectral bands (Inzana et al., 2003), making it easier to identify and analyze them (Inzana et al., 2003). In this research, one band ratio and three spectral indices were used in order to identify and reveal the iron oxide minerals in the studied site (Table 1).

2.4. RESULTS

2.4.1. PRINCIPAL COMPONENT ANALYSIS

In this section, the PCA as a data mining method, with the objective to minimize data redundancy and create new bands that will help to extract lineaments and identify the hydrothermal alteration areas. The Table 2 presents the eigenvalues of the different extracted principal components. The results showed that the first principal component can explain about 99.12 % of the data, which shows the very high effectiveness of the application of this method.

Figure 4a shows the color composition of the three first principal components (PC-1, PC-2, and PC-3) which represent the high percentage of information of the data, and Figure 4b shows the grey scale of the PC-1.

In addition to the PCA that has been applied for all bands, and to identify the iron oxides and hydrothermal areas, the PCA has been applied by selecting just four bands, focusing on those with the most absorption related to the targets (Table. 3). The Table 4 presents the correlation between the PCA and the selected bands. This helps to identify the principal component that contains more information about the target. The results show that the PC-1 represents a positive correlation with the difference selected bands, suggesting that this principal component presents more information about the hydrothermal alteration areas.

2.4.2. BAND RATIOS

In this section, the band ratio of the different spectral bands was extracted. The formula of these indices was chosen based on the reflectance and the absorption of the iron minerals and the hydrothermal alteration. Figure 5 presents the band ratio and the spectral indices in grey scale, a) 4/2, b) (4/2)*((4+6)/5), c) (3+6)/(4+5), and d) (2/1)-(5/4). The high value presents the area with iron and hydrothermal alteration.

Table 3 Selected bands of Landsat 9 sensor dataset to perform PCA method.

Sensor	Iron/OH-bearings	Selected bands
Landsat 9	Hydrothermal alterations	2, 5, 6 and 7
	Iron oxides	2, 4, 5 and 6

Table 4 Eigenvector matrix of PCA for selected bands of all sensor-type data to reveal different alterations.

Sensor	Iron/OH-be0arings	Eigenvector	Band 2	Band 5	Band 6	Band 7
Landsat 9	Hydrothermal alterations	PC 1	0.242041	0.525250	0.625573	0.523629
		PC 2	0.916237	0.128550	-0.358602	-0.124050
		PC 3	0.265378	-0.829515	0.230570	0.433955
		PC 4	-0.177481	0.139617	-0.653376	0.722570
	Iron/OH-bearings	**Eigenvector**	**Band 2**	**Band 4**	**Band 5**	**Band 6**
	Iron oxide	PC 1	0.256524	0.433512	0.556674	0.660588
		PC 2	0.778987	0.320544	0.029934	-0.538084
		PC 3	0.475232	-0.213122	-0.674279	0.523527
		PC 4	-0.318635	0.814799	-0.484320	-0.002846

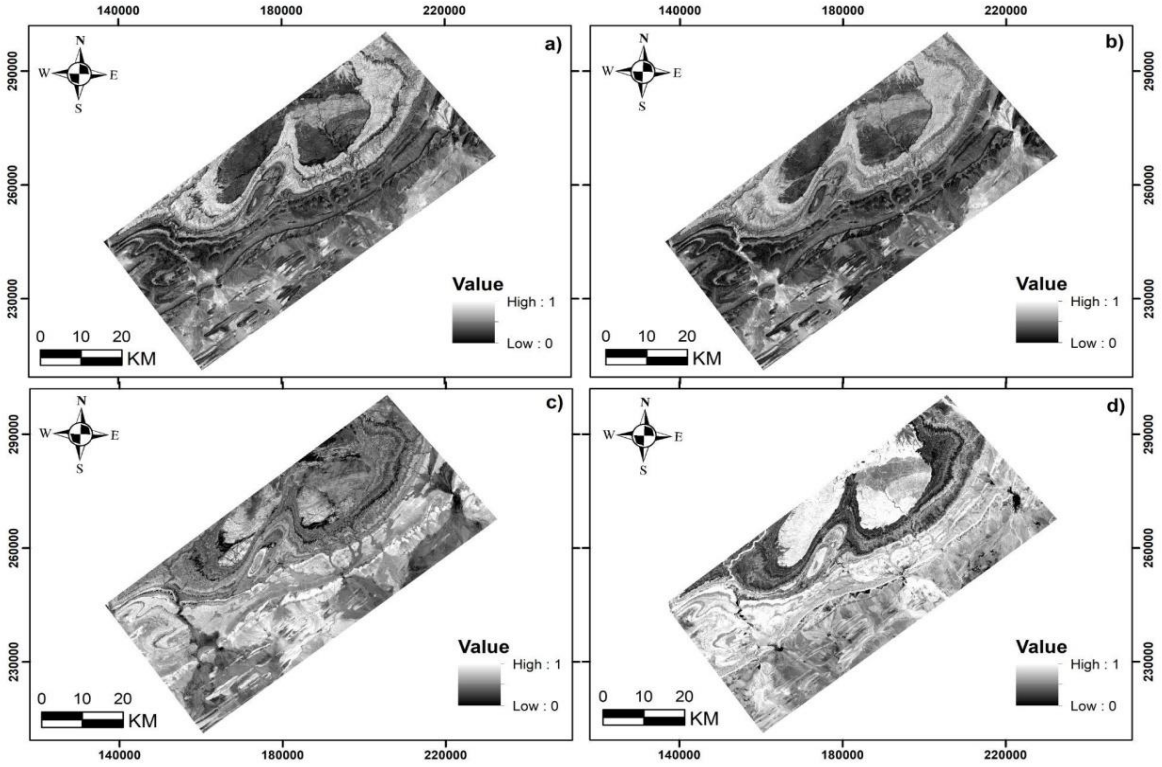

Fig. 5 Band ratio, a) 4/2, b) (4/2)*((4+6)/5), c) (3+6)/(4+5), and d) (2/1)-(5/4).

2.4.3. IRON OXIDES ALTERATION

Figure 6 shows the spatial distribution of iron oxide anomalies derived from the combined information extracted from PCA, band ratio analysis, and the spectral iron index using Landsat 9 data. Iron oxide anomalies are displayed together with extracted structural lineaments, and mineral index locations (Fe, Cu, Pb) obtained from field investigations and used for validation.

2.4.4. FIELD INVESTIGATIONS

Field validation was conducted through targeted sampling of remote-sensing-derived alteration zones. Approximately 38 field observation points corresponding to mineralized outcrops were collected during field investigations in the Foum Zguid and Fam El Hisn areas and projected onto the alteration map (Fig. 6). The spatial coincidence between these mineralized sites and the mapped alteration zones supports the geological relevance of the proposed approach.

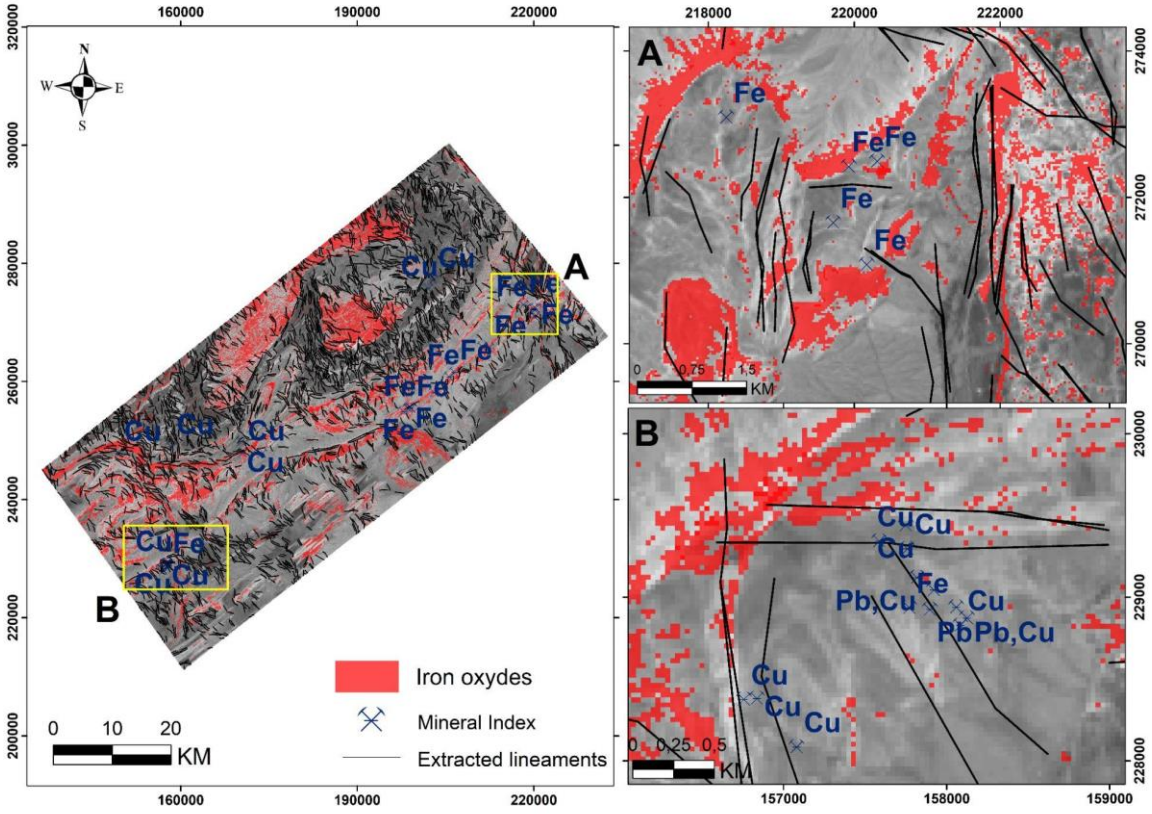

Fig. 6 Gossanic zones delineated from Landsat 9 OLI data.

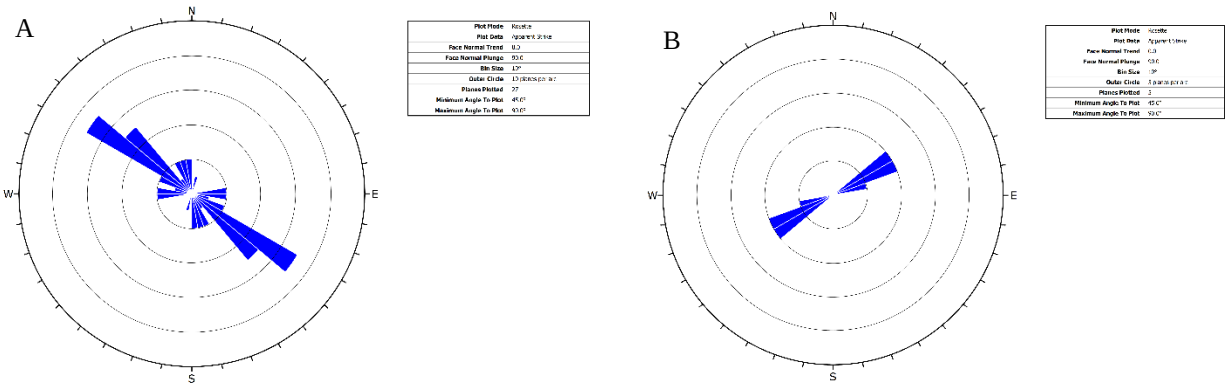

Fig. 7 Rose diagram of mineralized veins; A: Fam El Hisn area, B: Foum Zguid area.

The combination of the results obtained from the applied remote sensing techniques and the field observations highlights the consistency between alteration maps and ground truth data. Applying these techniques facilitates the delineation of potential mineralization zones and improves the efficiency of regional-scale exploration.

These two regions have significant exposures of minerals such as malachite, chalcopyrite, galena and in some areas iron oxide. For instance, the Foum Zguid area reveals the existence of lead mineralization (Fig. 8) and iron oxide (hematite) which is also visible at the surface. While, Fam El Hisn region shows a polymetallic mineralization, including Copper, Iron and Lead (Figs. 9 and 10) associated with iron oxide and quartz veins. These results demonstrate the effectiveness of remote sensing for mapping alteration zones and offer valuable insights for identifying new targets and optimizing mineral prospecting strategies.

The rose diagram of dip directions (Fig. 7) and Table 5 illustrate the distribution of the dominant vein orientations. In the Tata region, the mineralized veins are grouped into a family striking SE–NW to ESE–WNW (135° ± 10°) with subvertical dips. In the Foum Zguid region, the mineralized veins form a family striking NE–SW to ENE–WSW (65° ± 10°), also characterized by subvertical dips.

Table 5 Some structural measurements with a brief description of the mineralized veins.

Substance	Structural domain	Area	Ore-bodystructure	Strike, Dip and Dip Direction Ore-bodystructure
Pb,Cu	Western Anti-Atlas	Tata	Vein	N115-65NNE
Cu	Western Anti-Atlas	Tata	Vein	N145-75NE
Cu	Western Anti-Atlas	Tata	Vein	N25-87NW
Cu	Western Anti-Atlas	Tata	Vein	N120-80NNE
Cu	Western Anti-Atlas	Tata	Vein	N165-80WSW
Cu	Western Anti-Atlas	Tata	Veinlet	N155-90
Cu	Western Anti-Atlas	Tata	Vein	N175-88ENE
Pb	Western Anti-Atlas	Tata	Vein	N132-90
Cu	Western Anti-Atlas	Tata	Vein	N145-90
Pb,Cu	Western Anti-Atlas	Tata	Vein	N125-90
Pb,Cu	Western Anti-Atlas	Tata	Vein	N135-90
Pb,Cu	Western Anti-Atlas	Tata	Vein	N130-80SW
Pb,Cu	Western Anti-Atlas	Tata	Vein	N130-90
Cu	Western Anti-Atlas	Tata	Vein	N160-60SW
Cu	Western Anti-Atlas	Tata	Vein	N125-85NE
Cu	Western Anti-Atlas	Tata	Vein	N170-75W
Fe	Western Anti-Atlas	Tata	Vein	N85-45NW
Fe	Western Anti-Atlas	Tata	Mass	E-W
Fe	Western Anti-Atlas	Tata	Layer	N50-25SE
Fe	Western Anti-Atlas	Tata	Lens	N100-65N
Fe	Western Anti-Atlas	Tata	Lens	N115-70NNE
Fe	Western Anti-Atlas	Tata	Lens	N175-53W
Fe	Western Anti-Atlas	Tata	Vein	N94-64N
Fe	Western Anti-Atlas	Tata	Vein	N135-75NE
Fe	Western Anti-Atlas	Tata	Vein	N135-75NE
Fe	Western Anti-Atlas	Tata	Lens	N125-65NE
Fe	Western Anti-Atlas	Tata	Vein	N110-60NE
Fe	Western Anti-Atlas	Tata	Vein	N130-64NE
Fe	Western Anti-Atlas	Tata	Vein	N20-65W
Fe	Western Anti-Atlas	Tata	Vein	N140-60E
Fe	Western Anti-Atlas	Tata	Mass	N130-64NE
PB, Cu	Central Anti-Atlas	Foum Zguid	vein	N75-80NNW
Quartz	Central Anti-Atlas	Foum Zguid	veinlets	N55-70NNW
Quartz	Central Anti-Atlas	Foum Zguid	Vein locally brecciated	N55-75SE
Quartz	Central Anti-Atlas	Foum Zguid	Brecciated vein	N70-87NNW
Pb	Central Anti-Atlas	Foum Zguid	vein	N70-74S

2.5. DISCUSSION

The integration of multispectral remote sensing data, particularly through the application of Landsat 9 imagery, has proven highly effective for delineating hydrothermal alteration zones in the Tata region. The principal component analysis (PCA) method demonstrated exceptional data compression capabilities, with PC1 alone accounting for over 99 % of the spectral variance, confirming its suitability for highlighting mineralogical significant features.

The results indicate that band combinations sensitive to ferric and ferrous iron absorption features (especially bands 2, 4, 5, and 6); according to established approaches by (Sabins, 1999) and (Ito et al., 2022), are essential in revealing iron oxide anomalies, consistent with previous findings in similar metallogenic provinces e.g., (Abrams et al., 1983; Adiri et al., 2016). Band ratio techniques such as 4/2, (3+6)/(4+5) and composite indices like (4/2)*((4+6)/5) provided enhanced spectral contrast for identifying gossan and mineralized zones, reinforcing their practical utility in early-stage mineral exploration. Field validation in the Foum Zguid and Fam El Hisn areas confirmed the spectral data interpretations, as the identified alteration zones correlated with surface mineral occurrences including hematite, malachite, chalcopyrite, and galena. The spatial association between high lineament densities and mineralization further supports the role of structural controls in ore deposition.

Fig. 8 Lead mineralization in some mining trenches in the Foum Zguid area.

These results align with prior research conducted in the Anti-Atlas range and highlight the value of integrating remote sensing with geological fieldwork to improve the accuracy and efficiency of mineral prospecting. Preliminary tests using Sentinel-2 imagery produced alteration maps comparable to those obtained from Landsat 9; therefore, only Landsat 9 results are presented here to avoid redundancy. The positive correspondence between spectral signatures and on-ground mineralization underlines the reliability of remote sensing for regional exploration strategies in structurally complex terrains like the Anti-Atlas. Nevertheless, the 30 m spatial resolution of Landsat 9 may limit the detection of narrow mineralized veins or small gossans, and iron oxide anomalies may locally include non-hydrothermal iron staining or soil-related signals. Future work could benefit from the integration of complementary datasets, such as drone-based high-resolution imagery and geochemical sampling, to refine mineral discrimination and validation.

The main orientations of mineralized veins are grouped around N130–N140 in the Tata region. These orientations are typical of a compressive or transpressive regime, probably related to NE–SW-trending folding and to the reactivation of reverse faults during the Hercynian shortening. This tectonic phase also led, during the uplift of the Bas Drâa basement, to the development of SE-verging thrusts.

In the Foum Zguid region, the main orientations mineralized veins are grouped around N65–N70. These orientations are characteristic of a compressive or transpressive regime, likely associated with WNW–ESE-trending folding and the reactivation of reverse faults in the Central Anti-Atlas.

Fig. 9 Copper and Lead mineralization in the alteration zone at the Fam El Hisn area**.**

The mineralized veins crosscutting the Paleozoic formations are aligned along consistent structural directions, suggesting a common tectonic control in both regions. The Pb–Cu mineralization is concentrated along the most open fractures (generally SE–NW à ESE–WNW in Tata area et NE–SW à ENE–WSW in Foum Zguid area). The steeply dipping planes (dip > 70°) indicate subvertical veins, consistent with brittle fractures formed during late Hercynian deformation.

3. CONCLUSION

This study demonstrates the effectiveness of Landsat 9 multispectral imagery combined with band ratio techniques, principal component analysis, and structural lineament mapping for regional-scale hydrothermal alteration mapping in the Tata region. The applied approach successfully delineated iron oxide and iron sulphate related alteration zones, particularly in the Foum Zguid and Fam El Hisn areas. Field validation confirmed that the majority of the identified alteration zones correspond to surface mineralization, including copper, lead, and iron-bearing assemblages, supporting the geological relevance of the remote-sensing-derived targets. The study underlines the usefulness of remote sensing and field data to optimize mineral exploration efforts, reducing time and costs while improving precision. The successful delineation of alteration zones provides a valuable foundation for future exploration

Fig. 10 Gossanic zones with iron oxide mineralization in the alteration zone at the Fam El Hisn area.

campaigns and underscores the importance of integrating remote sensing with traditional geological survey techniques.

Structural analysis revealed that mineralization is preferentially associated with dominant fracture systems oriented SE–NW to ESE–WNW in the Fam El Hisn area and NE–SW to ENE–WSW in the Foum Zguid area, highlighting the strong structural control on ore localization.

This study confirms the suitability of Landsat 9 multispectral data for hydrothermal alteration mapping. The alignment between remote sensing results and the 38 field observations points validates the effectiveness of Landsat 9 as a cost-efficient dataset for regional-scale mineral exploration, particularly in structurally complex terrains like the Anti-Atlas. Future research utilizing higher-resolution remote sensing data could enhance the precision of target delineation for detailed exploration.

DECLARATION OF COMPETING INTEREST

The authors declare that they have no known competing financial interests or personal relationships that could have appeared to influence the work reported in this paper.

REFERENCES

Abia, E.H., Benssaou, M., Abioui, M., Ettayfi, N., Lhamyani, B., Boutaleb, S. and Barry Maynard, J.: 2020, The Ordovician Iron Ore of the Anti-Atlas, Morocco: Environment and dynamics of depositional process. Ore Geol. Rev., 120, 103447. DOI: 10.1016/j.oregeorev.2020.103447

Abrams, M.J., Ashley, R.P., Rowan, L.C., Goetz, A.F. and Kahle, A.B.: 1977, Mapping of hydrothermal alteration in the Cuprite mining district, Nevada, using aircraft scanner images for the spectral region 0.46 to 2.36 μm. Geology, 5, 12, 713–718. DOI: 10.1130/0091-7613(1977)5

Abrams, M.J., Brown, D., Lepley, L. and Sadowski, R.: 1983, Remote sensing for porphyry copper deposits in southern Arizona. Econ. Geol., 78, 4, 591–604. DOI: 10.2113/gsecongeo.78.4.591

Adiri, Z., Harti, A.E., Jellouli, A., Maacha, L. and Bachaoui, E.M.: 2016, Lithological mapping using Landsat 8 OLI and Terra ASTER multispectral data in the Bas Drâa inlier, Moroccan Anti Atlas. J. Appl. Remote Sens., 10, 1, 016005. DOI: 10.1117/1.JRS.10.016005

Adiri, Z., El Harti, A., Jellouli, A., Maacha, L., Azmi, M., Zouhair, M. and Bachaoui, E.M.: 2020, Mapping copper mineralization using EO-1 Hyperion data fusion with Landsat 8 OLI and Sentinel-2A in Moroccan Anti-Atlas. Geocarto Int., 35, 7, 781–800. DOI: 10.1080/10106049.2018.1544287

Álvaro, J., Benharref, M., Destombes, J., Carlos Gutiérrez-Marco, J., Hunter, A.W., Lefebvre, B., Van Roy, P. and Zamora, S.: 2022, Ordovician stratigraphy and benthic community replacements in the eastern Anti-Atlas, Morocco. Geol. Soc. Lond. Spec. Publ., 485, 1, SP485.20. DOI: 10.1144/SP485.20

Askkour, F., Saintilan, N.J., Madi, A., Chelle-Michou, C., Souhassou, M., Nourissaid, I., Ousbih, M., Spangenberg, J.E., Maacha, L. and Ikenne, M.: 2023, A lower Cambrian Moroccan Copperbelt? (Tizert copper deposit, Igherm inlier Anti Atlas, Morocco): preliminary results of Cu-Fe-sulfide Re-Os geochronology and stable sulfur isotope data. In: Proceedings of the 17th SGA Biennial Meeting, 2, 272–275.

Bahrami, Y., Hassani, H. and Maghsoudi, A.: 2021, Investigating the capabilities of multispectral remote sensors data to map alteration zones in the Abhar area, NW Iran. Geosyst. Eng., 24, 1, 18–30.

Belfoul, M.A., Faik, F. and Hassenforder, B.: 2001, Evidence of tangential tectonics prior to the major folding in the Hercynian chain of the western Anti-Atlas, Morocco. J. Afr. Earth Sci., 32, 723–739, (in French).

Bouchta, R., Boyer, F., Routhier, P., Saadi, M. and Salem, M.: 1977, The copper-bearing area of the Anti-Atlas (Morocco): permanence and rich ridges. C. R. Acad. Sci., Paris, 284, 503–506, (in French).

Broothaers, L.: 1977, Metallogenetic study of the Ordovician oolitic iron ore from Imi-Ntourza (southern Morocco). Notes et mémoires du Service géologique, 263, 116 pp, (in French).

Bruno, R., Kasmaeeyazdi, S., Tinti, F., Mandanici, E. and Balomenos, E.: 2021, Spatial component analysis to improve mineral estimation using Sentinel-2 band ratio: Application to a Greek bauxite residue. Minerals, 11, 6, 549. DOI: 10.3390/min11060549

Choubert, G.: 1963, Geological history of the Precambrian of the Anti-Atlas. Notes Mémoires Service Géologique Maroc, 162, 1–352, (in French).

Choubert, G. and Termier, H.: 1947, On the stratigraphy of the Moroccan Ordovician. Comptes Rendus sommaires des séances de la Société géologique de France, 16, 335–337, (in French).

Choubert, G.: 1943, The Acadian and Ordovician of the Anti-Atlas. C. R. Acad. Sci. Paris, 216, 1092–1094, (in French).

Choukrad, J., Ali, A.A., Mhamdi, H.S., Ouahzizi, Y., El Moutaouakkil, N., Saoud, N. and Charroud, M.: 2023, Contribution of Landsat 8 OLI imagery to mapping of lithological series and lineaments: implications for Pb-Zn mineralization exploration in the Boudahar Massif, Eastern High Atlas, Morocco. Estud. Geol., 79, 2, e159-e159. DOI: 10.3989/egeol.45041.1056

Courba, S., Hahou, Y., Achmani, J., Ouallali, A., El Amrani, M., Boudad, L., Idrissi, A., Aafir, Z., Sassioui, S., Ousaid, L., Ghadi, T., Lamchaimech, A. and Ben Driss Moulay, A.: 2023, Litho-structural and hydrothermal alteration mapping for mineral prospection in the Maider basin of Morocco based on remote sensing and field investigations. Remote Sens. Appl.: Soc. Environ., 31, 100980.
DOI: 10.1016/j.rsase.2023.100980

Crosta, A.P., De Souza Filho, C.R., Azevedo, F. and Brodie, C.: 2003, Targeting key alteration minerals in epithermal deposits in Patagonia, Argentina, using ASTER imagery and principal component analysis. Int. J. Remote Sens., 24, 21, 4233–4240.
DOI: 10.1080/0143116031000152291

Desthieux F.: 1977, Tectonic and metallogenic study of Jbel Addana, Ordovician of the Dra plains, pre-Saharan Morocco. Notes et memories Ser. géologiques Maroc, 268, 38, 209–236, (in French).

Destombes, J., Hollard, H. and Willefert, S.: 1985, Lower Palaeozoic rocks of Morocco. In: Holland, C.H. (Ed.), Lower Palaeozoic rocks of North-Western and West-Central Africa. John Wiley, Chichester, 91, 336 pp.

Destombes, J.: 1971, The Ordovician of Morocco: An attempt at stratigraphic synthesis. Mémoire, BRGM 73, 237–263, (in French).

Destombes, J.: 1963, The oolitic iron deposits of Imi n Tourza. Geological study. Rapport n° 763, SEGM Rabat, inedit. 77 pp, (in French).

Donzeau, M.: 1974, The Arc of the Anti-Atlas-Ougarta (north-western Sahara, Algeria-Morocco). C. R. Acad. Sci., Paris, 278, 417–420, (in French).

El Atillah, A., El Morjani, Z.E.A. and Souhassou, M.: 2019, Use of Landsat 7 and 8 multispectral imagery for mineral exploration: The case of the Bou-Azzer-El Graara inlier, Morocco. Int. J. Innov. Appl. Stud., 28, 1, 299–315, (in French).

El Basbas, A., Aissa, M., Ouguir, H., Mahdoudi, M.L., Madi, A. and Zouhair, M.: 2020, Ouansimi copper mineralization (Western Anti-Atlas, Morocco): paragenetic sequence and circulation of gangue hosted paleofluids. J. Afr. Earth Sci., 162, 103692.
DOI: 10.1016/j.jafrearsci.2019.103692

El Ouad, Z., Belfoul, M.A., Souhassou, M., Ikenne, M., Nathwani, C., Ez-zghoudy, M. and El Atillah, A.: 2025, Lithostructural controls of Pb-Cu-Ag mineralized veins of Jbel Addana district (Western Anti-Atlas, Morocco): Implications for mineral exploration. J. Afr. Earth Sci., 232, 105801.
DOI: 10.1016/j.jafrearsci.2025.105801

Faik, F.: 2005, Lithostratigraphy and structures of the central-western Anti-Atlas: from late-Proterozoic rifting to the Hercynian orogeny. Thèse d'Etat, Université Ibn Zohr, Agadir, Maroc, 242 pp., (in French).

Hajaj, S., El Harti, A., Jellouli, A., Pour, A.B., Mnissar Himyari, S., Hamzaoui, A. and Mazlan, H.: 2024, ASTER data processing and fusion for alteration minerals and silicification detection: Implications for cupriferous mineralization exploration in the western Anti-Atlas, Morocco. Artif. Intell. Geosci., 5, 100077.
DOI: 10.1016/j.aiig.2024.100077

Hassenforder, B.: 1987, The Pan-African and Variscan tectonics of the Anti-Atlas in the Kerdous massif (Morocco). Université L. Pasteur, Strasbourg, France. Thèse Scientifique, 249 pp., (in French).

Goetz, A.F., Rock, B.N. and Rowan, L.C.: 1983, Remote sensing for exploration; an overview. Econ. Geol., 78, 4, 573–590. DOI: 10.2113/gsecongeo.78.4.573

Gutiérrez-Marco, J.C., Sá, A.A., Álvaro, J.J., Rábano, I., Zamora, S., Colmenar, J., Pereira, S. and García-Bellido, D.C.: 2019, A correlation of the Ordovician of the Anti-Atlas (Morocco) with reference to the global and regional chronostratigraphic scales. Società Geologica Italiana, 3rd International Congress on Stratigraphy (STRATI 2019), Milano, 2-5 July 2019. http://hdl.handle.net/10261/204866

Inzana, J., Kusky, T., Higgs, G. and Tucker, R.: 2003, Supervised classifications of Landsat TM band ratio images and Landsat TM band ratio image with radar for geological interpretations of central Madagascar. J. Afr. Earth Sci., 37, 1-2, 59–72.
DOI: 10.1016/S0899-5362(03)00071-X

Ito, G., Flahaut, J., González-Maurel, O., Godoy, B., Payet, V. and Barthez, M.: 2022, Remote sensing survey of altiplano-puna volcanic complex rocks and minerals for planetary analog use. Remote Sens., 14, 9, 2081. DOI: 10.3390/rs14092081

Kariuki, P.C., Woldai, T. and Van Der Meer, F.: 2004, Effectiveness of spectroscopy in identification of swelling indicator clay minerals. Int. J. Remote Sens., 25, 2, 455–469. DOI: 10.1080/0143116031000084314

Kharis, A., Aissa, M., Baidder, L., Ouguir, H., Mahdoudi, M.L., Zouhair, M. and Ouadjou, A.: 2011, Oumjrane-Bou Nahas, a Copper Mine in the Maider Upper Ordovician Quartzites. Notes et mémoires Serv. Géol., 564, 9, 65–71, (in French).

Kruse, F.A., Lefkoff, A.B., Boardman, Y.J., Heidebrecht, K.B., Shapiro, A.T., Barloon, P.J. and Goetz, A.F.H.: 1993, The spectral image processing system (SIPS)–interactive visualization and analysis of imaging spectrometer data. Remote Sens. Environ., 44, 2-3, 145–163.

Lefebvre, B., El Hariri, Kh., Lerosey-Aubril, R., Servais, Th. and Van Roy, P.: 2015, The Fezouata Shale (Lower Ordovician, Anti-Atlas, Morocco): a historical review. Palaeogeogr. Palaeoclimatol. Palaeoecol., 460, 7–23. DOI: 10.1016/j.palaeo.2015.10.048

Loughlint, W.P.: 1991, Principal component analysis for alteration mapping. Photogramm. Eng. Remote Sens., 57, 9, 1163–1169. DOI: 10.1080/01431160600905003

Mattauer, M., Proust, F. and Taponnier, P.: 1972, Major strikeslip fault of a late hercynien age in Morocco. Nature, 237, 160–162. DOI: 10.1038/237160b0

Michard, A., Saddiqi, O., Chalouan, A. and De Lamotte, D.F.: 2008, Continental evolution: The Geology of Morocco, 438 pp.

Ouchchen, M., Boutaleb, S., Hassan, E., El, D., Abioui, M., Mickus, K.L., Miftah, A., Zahra, F. and Dadi, B.: 2021, Structural interpretation of the Igherm region (western anti atlas, Morocco) from an aeromagnetic analysis: implications for copper exploration. J. Afr. Earth Sci., 176, 104140. DOI: 10.1016/j.jafrearsci.2021.104140

Oummouch, A., Essaifi, A., Zayane, R., Maddi, O., Zouhair, M. and Maacha, L.: 2017, Geology and metallogenesis of the sediment-hosted Cu-Ag deposit of Tizert (Igherm Inlier, Anti-Atlas Copperbelt, Morocco). Geofluids, 3, 1–19. DOI: 10.1155/2017/7508484

Peña, S.A. and Abdelsalam, M.G.: 2006, Orbital remote sensing for geological mapping in southern Tunisia: implication for oil and gas exploration. J. Afr. Earth Sci., 44, 2, 203–219. DOI: 10.1016/j.jafrearsci.2005.10.011

Piqué, A., Bouabdelli, M. and Darboux, J.-R.: 1995, The Cambrian Rift of Western Morocco. C. R. Acad. Sci. Paris, 320, 1017–1024, (in French).

Piqué, A. and Michard, A.: 1981, The structural zones of Hercynian Morocco. Sciences Géologiques Bulletin 34, 135146, (in French).

Pour, A.B. and Hashim, M.: 2015, Hydrothermal alteration mapping from Landsat-8 data, Sar Cheshmeh copper mining district, south-eastern Islamic Republic of Iran. J. Taibah Univ. Sci., 9, 2, 155–166. DOI: 10.1016/j.jtusci.2014.11.008

Pour, A.B., Hashim, M., Park, Y. and Hong, J.K.: 2018, Mapping alteration mineral zones and lithological units in Antarctic regions using spectral bands of ASTER remote sensing data. Geocarto Int., 33, 12, 1281–1306.

Pour, A.B., Rahmani, O. and Parsa, M.: 2023, Editorial for the Special Issue: "Multispectral Remote Sensing Satellite Data for Mineral and Hydrocarbon Exploration: Big Data Processing and Deep Fusion Learning Techniques. Minerals, 13, 2, 193. DOI: 10.3390/min13020193

Raddi, Y., Baidder, L., Rjimati, E.C. and Ait Brahim, L.: 2011, Imin'Tourza Oolithic Iron Deposit south of Jbel Saghro. Notes et mémoires Serv., 564, 9, 41–44, (in French).

Ranjbar, H., Honarmand, M. and Moezifar, Z.: 2004, Application of the Crosta technique for porphyry copper alteration mapping, using ETM+ data in the southern part of the Iranian volcanic sedimentary belt. J. Asian Earth Sci., 24, 2, 237–243. DOI: 10.1016/j.jseaes.2003.11.001

Rowan, L.C., Goetz, A.F. and Ashley, R.P.: 1977, Discrimination of hydrothermally altered and unaltered rocks in visible and near infrared multispectral images. Geophysics, 42, 3, 522–535. DOI:10.1190/1.1440723

Roy, D.P., Wulder, M.A., Loveland, T.R., Woodcock, C.E., Allen, R.G., Anderson, M.C., ..., Zhu, Z.: 2014, Landsat-8: Science and product vision for terrestrial global change research. Remote Sens. Environ., 145, 154–172. DOI: 10.1016/j.rse.2014.02.001

Sabins, F.F.: 1999, Remote sensing for mineral exploration. Ore Geol. Rev., 14, 3-4, 157–183. DOI: 10.1016/S0169-1368(99)00007-4

Singh, A. and Harrison, A.: 1985, Standardized principal components. Int. J. Remote Sens., 6, 6, 883–896. DOI: 10.1080/01431168508948511

Soulaimani, A., Michard, A., Ouanaimi, H., Baidder, L., Raddi, Y., Saddiqi, O. and Rjimati, E.C.: 2014, Late Ediacaran-Cambrian structures and their reactivation during the Variscan and Alpine cycles in the Anti-Atlas (Morocco). J. Afr. Earth Sci., 98, 94–112. DOI: 10.1016/j.jafrearsci.2014.04.025e

Soulaimani, A. and Burkhard, M.: 2008, The Anti-Atlas chain (Morocco): the southern margin of the Variscan belt along the edge of the West African craton. Geol. Soc. Spec. Publ., 297, 433–452. DOI: 10.1144/SP297.20

Soulaimani, A., Lecorre, C. and Farazdaq, R.: 1997, Hercynian deformation and basement/cover relationship in the Lower Drâa region (Western Anti-Atlas, Morocco). J. Afr. Earth Sci., 24, 3, 271–284, (in French). DOI: 10.1016/S0899-5362(97)00043-2

Sumrall, C.D. and Zamora, S.: 2011, Ordovician edrioasteroids from Morocco: faunal exchanges across the Rheic Ocean. J. Syst. Palaeontol., 9, 3, 425–454. DOI: 10.1080/14772019.2010.499137

Zeinelabdein, K.A.E. and El Nadi, A.H.: 2014, The use of Landsat 8 OLI image for the delineation of gossanic ridges in the Red Sea Hills of NE Sudan. J. South Am. Earth Sci., 1, 3, 62–67.

Zhang, X., Pazner, M. and Duke, N.: 2007, Lithologic and mineral information extraction for gold exploration using ASTER data in the south Chocolate Mountains (California). ISPRS J. Photogramm. Remote Sens., 62, 271–282. DOI: 10.1016/j.isprsjprs.2007.04.004